Electrochemical Studies of the Lateral Diffusion of TEMPO in the Aqueous Liquid/Vapor Interfacial Region

Nicolas Glandut,[†] Andrew D. Malec,[†] Michael V. Mirkin,[‡] and Marcin Majda*[,†]

Department of Chemistry, University of California, Berkeley, Berkeley, California 94720-1460, and Department of Chemistry and Biochemistry, Queens College-CUNY, Flushing, New York 11367

Received: December 5, 2005; In Final Form: January 19, 2006

Surface partitioning and lateral mobility of TEMPO (2,2,6,6-tetramethyl-1-piperidynyloxy free radical) in the aqueous liquid/gas interfacial region were investigated electrochemically with 100 nm wide, 1.0 cm long microband electrodes positioned at the air/water interface. For redox active amphiphiles such as TEMPO, the electrochemical current is the sum of the surface and solution components representing the diffusive transport of TEMPO in both domains as well as the dynamics of equilibration at the air/water interface. Interpretation of the recorded current−voltage curves was aided by a FEMLAB simulation code developed to analyze transport processes in this class of systems. TEMPO and $TEMPO^+$ partition constants (K_T, K_{T^+}) and solution diffusivities (D_{sol}, equal for the two species) were obtained experimentally yielding $K_T = 5.0 \pm 0.7 \times 10^2$ M^{-1}, $K_{T+} = 41 \pm 3$ M^{-1}, and $D_{sol} = 7.7 \pm 0.35 \times 10^{-6}$ cm^2/s. In view of the low value of K_{T^+}, $TEMPO^+$ was assumed not to partition to the air/water interface. We further assumed that the desorption rate constants (k_{des}) of both TEMPO and $TEMPO^+$ were the same. Good fits between the recorded and simulated cyclic voltammograms were obtained using two correlated, adjustable parameters, k_{des} and the TEMPO lateral, surface diffusion constant (D_{surf}). Detailed analysis of the behavior of this class of systems was obtained for a broad range of D_{surf} and k_{des} values. In addition, a calibration curve of k_{des} versus D_{surf} was obtained. Assuming that TEMPO k_{des} is in a likely range of 10−100 s^{-1}, its lateral diffusion constant is in the range of $7.9-3.6 \times 10^{-5}$ cm^2/s. In view of our earlier work (Wu, D. G.; Malec, A. D.; Head-Gordon, M.; Majda, M. *J. Am. Chem. Soc.* **2005**, *127*, 4490−4496) showing that at the air/water interface TEMPO is unimmersed, and that its interactions with water are limited to hydrogen bonding with one or two water molecules, D_{surf} can be related to the viscosity of the aqueous interfacial region.

Introduction

Structural and dynamic properties of the aqueous liquid/vapor interfacial region are of considerable importance and constitute a focal point of recent experimental and theoretical research. Abundance of water on our planet and in its atmosphere as well as the importance of water in all environmental and biological processes more than adequately explain and justify these interests. Essentially all recent experimental investigations of the aqueous interfacial region concerned its structural properties. In particular, modern spectroscopic methods such vibrational sum frequency spectroscopy,[1−5] X-ray reflectivity,[6,7] and EXAFS[8] revealed structural details of the water interfacial region such as its width, the extent of hydrogen bonding, and the orientational distribution of the water molecules. In parallel with those investigations, a number of theoretical studies involving molecular dynamics calculations offered further insights, including assessment of the dynamic properties of the aqueous interfacial region such as hydrogen-bond dynamics and the water lateral diffusion constant near and within the interfacial region.[9−17] These theoretical results are particularly valuable since experimental characterization of the dynamic properties of water in this crucial region have not, by and large, been available. Our recent experimental work is intended to address this problem.[18]

Our approach involves electrochemical measurements of the lateral diffusion of a probe species along the air/water interface.[19] We showed recently that TEMPO (2,2,6,6-tetramethyl-1-piperidynyloxy free radical) is a particularly suitable probe in these

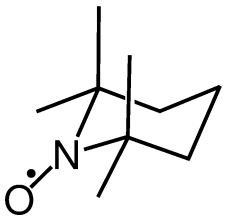

investigations.[18] Its structure features a redox active nitroxide group which is a part of the six-membered piperidine ring and which is surrounded by four methyl groups. This highly hydrophobic, sterically shielding environment around the polar nitroxide group determines the extent of TEMPO−water interactions at the air/water interface. TEMPO is, indeed, a surfactant partitioning to the water surface with the equilibrium constant, $K = 5.0 \pm 0.7 \times 10^2$ M^{-1}. Our electronic structure calculations showed that a single water molecule forms a hydrogen bond with TEMPO that is approximately 30% stronger than the H_2O-H_2O hydrogen bond.[18] These calculations led us to postulate that TEMPO diffuses along the interface largely unimmersed and that it is coupled to the interfacial water via

* Corresponding author. Fax: (510) 642-0269. E-mail: majda@berkeley.edu.
[†] University of California.
[‡] Queens College-CUNY.

10.1021/jp0570824 CCC: $33.50
Published on Web 03/07/2006

hydrogen bonding. This particular feature of TEMPO−water interactions makes TEMPO a uniquely suitable probe of the water interfacial region. Indeed, the measured lateral diffusion constant of TEMPO ($D_{surf} = 1.5 \pm 0.7 \times 10^{-4}$ cm^2/s) obtained for TEMPO surface concentrations below 15% full monolayer coverage can be taken as an approximation of the diffusion constant of water in the interfacial region. In view of this, we estimated the viscosity of the aqueous liquid/vapor interfacial region to be as much as 4 times smaller than that of bulk liquid water.[18]

Electrochemistry of TEMPO at the air/water interface presents a rather complex problem since TEMPO is a water-soluble probe, and therefore, diffusion processes both along the interface and in the bulk water must be simultaneously considered. In addition, partition thermodynamics and kinetics of both TEMPO (T) and its one-electron oxidation product, TEMPO oxonium cation (T^+), must be also included in the interpretation of the observed current−voltage curves in order to extract the TEMPO interfacial, lateral diffusion constant. The electrochemical experiments mentioned here were carried out with line microelectrodes positioned in the plane of the air/water interface. Total current in these experiments necessarily consists of two components due to diffusion of TEMPO along the air/water interface and in the bulk. In the previous report, we developed a technique in which the water surface could be coated by a compact monolayer of stearic acid, a nonelectrochemically active, insoluble amphiphile.[18] This prevents TEMPO partitioning to the air/water interface. Under these circumstances, the measured current represents only the bulk population of TEMPO. We argued that subtraction of that current from the total current recorded in the absence of the stearic acid monolayer approximated the surface current due to the lateral diffusion of TEMPO on the water surface. This approach becomes exactly correct in the limit of negligibly slow kinetics of TEMPO partitioning at the air/water interface. Since the rate of TEMPO partitioning is not known and cannot be assumed to be negligibly slow, the resulting TEMPO D_{surf} values were not fully accurate. We now present a more detailed analysis of TEMPO electrochemistry at the air/water interface that explicitly treats both bulk and surface diffusive fluxes and the kinetics of TEMPO interfacial partitioning. We rely on finite element simulations of the total cyclic voltammetric current. We show that the shape and the magnitude of the simulated voltammograms depend on two experimental parameters, D_{surf} and the rate constant of TEMPO desorption from the water surface, k_{des}. We rely on the measured value of the TEMPO partition constants ($K = 5.0 \pm 0.70 \times 10^2$ M^{-1}). We established that T^+ partitioning to the air/water interface is negligible ($K_{T^+} = 41 \pm 3$ M^{-1}). In addition, we consider the effect of the water meniscus formed near the line electrode when it touches the interface. Our major conclusion is that for a likely range of TEMPO desorption rate constants of 10−100 s^{-1}, its lateral surface diffusion constant is in the range $7.9-3.6 \times 10^{-5}$ cm^2/s, or somewhat lower than the 1.5×10^{-4} cm^2/s reported previously.

Experimental Section

Reagents. TEMPO, 4-hydroxy-TEMPO, lithium perchlorate, calcium hypochlorite, 1-octadecanethiol (OM), and octadecyltrichloro-silane (OTS) were purchased from Aldrich. Perchloric acid and diethyl ether were purchased from EM Industries, Inc. (Merck). Tetrafluoroboric acid was purchased from Fisher. All these chemicals were used as received without further purification. Millipore Milli-Q water (18 MΩ cm) was used in all experiments.

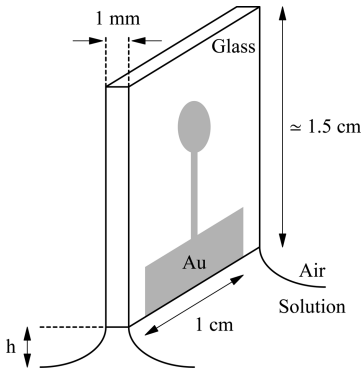

Figure 1. Drawing showing a line microband electrode touching the air/water interface. Its position relative to the water surface is described by the meniscus height, *h*. The shaded area corresponds to a 100 nm thick, vapor-deposited gold film. The line electrode fabrication procedure is outlined in the Experimental Section.

Synthesis of TEMPO−BF_4. The tetrafluoroborate salt of $TEMPO^+$ was prepared following the procedure of Bobbitt and co-workers[20−22] and Golubev et al.[23] Briefly, 2 equiv of HBF_4 50% were added to a solution of 0.032 mol of TEMPO in 5 mL of diethyl ether. The reaction mixture was cooled to 0 °C and stirred for 2 h. The yellow precipitate was filtered and collected. Then, 0.5 equiv of ClO^- (0.008 mol of $Ca(ClO)_2$) was added to the filtrate, and again the reaction was cooled to 0 °C and stirred for 2 h. The precipitate was filtered. The two precipitates were recrystallized from H_2O. The measured melting point of 163 ± 1 °C matches the literature value of 163.0 ± 0.5 °C.[23] Elemental analysis results calculated for $C_9H_{18}NOBF_4$ (w%): C = 44.4, H = 7.4, and N = 5.8. Found: C = 44.2, H = 7.5, and N = 5.6.

Fabrication of the Line Microelectrodes. The fabrication procedure was given in our earlier papers.[19,24,25] We introduce one modification to that procedure: a 5 nm thick, vapor-deposited Cr film was used instead of 3-mercaptopropyltrimethoxy-silane as a means of enhancing the stability of the gold films. Briefly, $w = 100$ nm thick gold films were vapor deposited on 1 mm thick glass slides (surface area, 3×1 in^2) immediately following a 5 nm Cr film deposition. Monolayers of OM and OTS were then sequentially formed on gold and glass, respectively, to render these surfaces hydrophobic. Breaking these electrode substrates in half creates two microband electrodes at the hydrophilic cross section of the gold-coated glass slide (see Figure 1). Immediately afterward, one of these microelectrodes is positioned at the air/water interface by touching the water surface with the newly created, clean edge of a fractured glass slide. A sharp gradient of wettability at the edge between the OM-coated and clean gold is thus formed and functions as a line electrode for the redox species diffusing along the air/water interface. The freshly generated cross-sectional area of the vapor-deposited gold film is exposed to the aqueous solution and functions as a 100 nm wide microband electrode for the redox species in the bulk of solution. We note that, while prior to fracturing electrode substrates can be stored in an evacuated desiccator essentially indefinitely without any detrimental effects, once fractured, a line electrode must be used immediately. For this reason, the other half of the fractured electrode substrate was discarded.

Electrochemical Measurements. All cyclic voltammograms were recorded with a CH Instruments 660B potentiostat (Austin, TX), in a ca. 1 cm deep, circular (with diameter of ca. 7 cm), homemade Teflon dish. The positioning of a line microelectrode at the air/water interface (and therefore the curvature of the liquid meniscus; see Figure 1) was precisely controlled with a

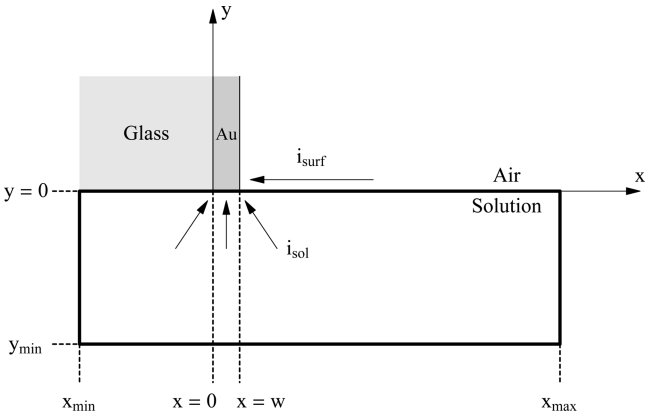

Figure 2. Side-view diagram of the microband electrode at the air/water interface. The microband width, *w*, is 100 nm. The thick line rectangle outlines the dimensions of the FEMLAB simulation domain (see details in the Experimental Section).

Mitutoyo height gauge (model 192-116). With this apparatus, the height of the electrode above the water surface can be adjusted with a 25 μm precision. The aqueous solution (50 mM $LiClO_4$, 1 mM $HClO_4$ at 25 °C) diffusion constants, D_{sol}'s, of TEMPO and its derivatives were measured using a calibrated 3.25 μm radius Au microdisk electrode. These were (all $\times 10^{-6}$ cm^2/s) TEMPO = 7.7 ± 0.35, $TEMPO^+$ = 8.0 ± 0.4, and 4-hydroxy-TEMPO = 7.1 ± 0.25. These values are in a very good agreement with those measured previously.[26,27]

Surface Tension Measurements. Surface pressure versus concentration curves for TEMPO and $TEMPO^+$ solutions were obtained using a CSC Scientific Company Inc. du Noüy tensiometer (model 70535; Fairfax, VA). The tensiometer's Pt ring was flamed between each experiment in order to remove organic impurities.

Digital Simulations. The finite element simulations of cyclic voltammograms were done with FEMLAB (version 3.1 with the Chemical Engineering module) on a Dell Precision workstation 650 running with a 2.8 GHz Xenon processor, using 2 GB RAM (OS, Red Hat Linux 8.0). We relied on FEMLAB's "Transport and Adsorption" weak-form model. The dimensions of the simulation domain, x_{min}, x_{max}, and y_{min}, (see Figure 2) were chosen according to the following:[28] $x_{min} = y_{min} = 6\sqrt{D_{sol}t_{end}}$, and $x_{max} = 6\sqrt{D_{surf}t_{end}}$, where D_{sol} and D_{surf} are the TEMPO diffusion constants in bulk solution and its maximum expected value on the water surface, respectively; t_{end} is the duration of a voltammetric scan. For more details see the following section. A mesh made of unstructured triangles was generated by using the built-in mesh generator with the default settings. This mesh was refined in a region near the microband electrode. Each simulation lasted approximately 300 s (5 min). Additional simulations of cyclic voltammograms due solely to the solution processes were done with DigiSim package (model 3.03aCV, Bioanalytical Systems Inc., West Lafayette, IN).

Theoretical Description and Results

We are concerned with the Nernstian, one-electron oxidation of TEMPO (T) to its oxonium cation, T^+ shown in Scheme 1.[18] The aqueous electrochemistry of the T^+/T couple was investigated by Fish et al. in a broad pH range of 2−12.[29] They measured the heterogeneous rate constant of this one-electron reaction to be 3.1×10^{-3} cm/s relying on the measurements of the voltammetric peak-to-peak separation ($E_{pa} - E_{pc}$) at scan rates above 0.1 V/s (the Nicholson and Shain method). At scan rates less or equal to 0.1 V/s, they determined the system to be

SCHEME 1

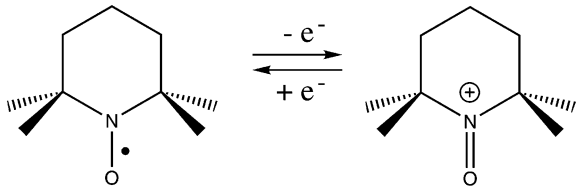

reversible exhibiting a Nernstian peak-to-peak separation of 60 ± 5 mV.[29] We have reexamined TEMPO reversibility in 50 mM $LiClO_4$, 1.0 mM $HClO_4$ electrolyte employed in the work described below using macroscopic (0.20 cm^2), vapor-deposited, gold on glass disk electrodes. By quantitatively determining that the anodic to cathodic peak separation of 68 ± 4 mV does not vary with the scan rate in the range of scan rates of 0.01−0.1 V/s, we confirmed the reversible behavior of this redox couple in this range of scan rates as originally reported by Fish et al. The measured value of the T^+/T formal redox potential is 0.49 ± 0.01 V versus SCE. The electrochemical reactions occur at a microband electrode touching the air/water interface. The latter is shown in Figure 1 and described in the Experimental Section. The height of the water meniscus adjacent to the microband is an adjustable parameter and affects the magnitude of the observed current. We discuss this in the Experimental Results and Discussion section. The measurements and the theoretical modeling were done for the conditions of zero meniscus height (see Figure 2). Since TEMPO partitions to the air/water interface, there exist two populations of TEMPO, on the water surface and in the solution. Both populations can be oxidized at the same potential. In other words their formal potentials are assumed to be the same. Thus, the measured current consists of the diffusion-limited components of the surface and solution populations of T. TEMPO diffusing along the water surface reacts at the line electrode ($y = 0$, $x = w$), and the T bulk population reacts at the microband electrode ($y = 0$, $0 < x < w$). Mass transport of T and T^+ in the solution phase is governed by the Fick's second law equation:

$$\frac{\partial C(x,y,t)}{\partial t} = D_{sol}\left[\frac{\partial^2 C(x,y,t)}{\partial x^2} + \frac{\partial^2 C(x,y,t)}{\partial y^2}\right] \qquad (1)$$

where the concentration function $C(x,y,t)$ and the diffusion constant D_{sol} refer to both T and T^+ species. Equation 1 is valid for $-\infty < x < +\infty$ and $-\infty < y < 0$. In view of the measurements reported in the Experimental Section, $D_{sol,T} = D_{sol,T^+} = D_{sol}$.

TEMPO partitioning to the air/water interface ($y = 0$ and $w \le x < +\infty$) is characterized by a partition constant ($K = 5.0 \pm 0.70 \times 10^2$ M^{-1}) which can be expressed by the ratio of the adsorption and desorption rate constants, $K = k_{ads}/k_{des}$, and obeys the Langmuir adsorption isotherm. The latter point was demonstrated in our previous report.[18]

$$\Gamma_{init} = \Gamma_{max}\frac{KC_{init}}{1 + KC_{init}} \qquad (2)$$

where Γ_{init} and C_{init} refer to the initial surface and bulk concentrations of T, respectively, and Γ_{max} is the surface concentration of the full monolayer ($\Gamma_{init} = 1.5 \pm 0.2 \times 10^{-11}$ mol/cm^2, $C_{init} = 0.1$ mM, $\Gamma_{max} = 3.2 \pm 0.2 \times 10^{-10}$ mol/cm^2). We determined experimentally that the partitioning of T^+ is very small. Thus, we assume that $K_{T^+} = 0$ and that T^+ formed electrochemically at the air/water interface desorbs with the same rate constant as T.

Mass transport of T and T^+ on the water surface is governed by the Fick's second law modified by the adsorption/desorption kinetics:

$$\frac{\partial \Gamma_T(x,t)}{\partial t} = D_{surf}\frac{\partial^2 \Gamma_T(x,t)}{\partial x^2} + k_{ads}C_T(x,0,t)\Gamma_\phi(x,t) - k_{des}\Gamma_T(x,t) \quad (3)$$

and

$$\frac{\partial \Gamma_{T^+}(x,t)}{\partial t} = D_{surf}\frac{\partial^2 \Gamma_{T^+}(x,t)}{\partial x^2} - k_{des}\Gamma_{T^+}(x,t) \quad (4)$$

where D_{surf} is the surface diffusion constant of T and T^+. In other words, we assume that the surface diffusion constants of T and T^+ are equal. While this simplifying assumption may not be rigorously correct, it is well justified in view of the TEMPO water interactions at the interface and the expected high desorption rate constant of T^+. In eq 3, Γ_ϕ is the surface concentration of the vacant adsorption sites: $\Gamma_\phi = \Gamma_{max} - \Gamma_T - \Gamma_{T^+}$. Equations 1, 3, and 4 were solved with the usual initial and boundary conditions.[30] Those bearing spatial characteristics of our system are listed below:

(1) for $t = 0$

$$C_T(x,y,t) = C_{init}, \quad \text{for} \quad -\infty < x < +\infty \quad \text{and} \quad -\infty < y < 0 \quad \text{(i)}$$

$$C_{T^+}(x,y,t) = 0, \quad \text{for} \quad -\infty < x < +\infty \quad \text{and} \quad -\infty < y < 0 \quad \text{(ii)}$$

$$\Gamma_T(x,t) = \Gamma_{init}, \quad \text{for} \quad w \le x < +\infty \quad \text{(iii)}$$

$$\Gamma_{T^+}(x,t) = 0, \quad \text{for} \quad w \le x < +\infty \quad \text{(iv)}$$

(2) for $t > 0$

$$\frac{C_{T^+}(x,y,t)}{C_T(x,y,t)} = \exp\left[\frac{F}{RT}(E - E^0)\right], \quad \text{for} \quad 0 < x < w \quad \text{and} \quad y = 0 \quad \text{(v)}$$

$$\frac{\Gamma_{T^+}(x,t)}{\Gamma_T(x,t)} = \exp\left[\frac{F}{RT}(E - E^0)\right], \quad \text{for} \quad x = w \quad \text{(vi)}$$

The microband currents due to TEMPO solution (i_{sol}) and surface (i_{surf}) mass transport are (refer to Figure 2):

$$i_{sol} = FlD_{sol}\int_0^w \left[\frac{\partial C_T(x,y,t)}{\partial y}\right]_{y=0} dx \quad (5)$$

$$i_{surf} = FlD_{surf}\left[\frac{\partial \Gamma_T(x,t)}{\partial x}\right]_{x=w} \quad (6)$$

where F is the Faraday constant and l is the length of the microband electrode. Naturally, the total current is $i_{tot} = i_{sol} + i_{surf}$.

Finite element simulations of cyclic voltammograms for this system were obtained for a set of parameters reflecting our experimental work discussed below. To reiterate, $D_{sol} = 7.7 \times 10^{-6}$ cm^2/s, $w = 100$ nm, $l = 1.0$ cm, scan rate $\upsilon = 20$ mV/s, $K = 504$ M^{-1}, and $\Gamma_{max} = 3.2 \times 10^{-10}$ mol/cm^2. The initial solution concentration of TEMPO was taken to be 0.10 mM which gave $\Gamma_{init} = 1.5 \times 10^{-11}$ mol/cm^2. The latter corresponds to 4.7% of the full monolayer coverage. In view of the system's description given above, the magnitude of the total current and of its two components is a function of just two unknown parameters: D_{surf} and k_{des}. The former is the key object of these investigations. The latter has not been measured for TEMPO. We can hypothesize that it is on the order of $10-100$ s^{-1}. For comparison, desorption rate constants for the following surfactants were reported in the literature: decanol, 220 s^{-1};[31] pentanol, 115 s^{-1};[32] heptanol, 110 s^{-1}.[32] In addition, Abbott and co-workers obtained the desorption rate constant for decanol of 45 s^{-1} using molecular dynamics simulations.[33]

To best understand the behavior of this class of systems, we carried out cyclic voltammetric simulations with k_{des} ranging from 10^{-2} to 10^2 s^{-1} and for D_{surf} values ranging from $^1/_{20}$ to 20 times D_{sol} given above. Representative results of these simulations are collected in Figure 3. While there exist numerous interesting features of this collection of current−voltage curves, we focus below on the following three most revealing and notable ones.

When the rate of surfactant equilibration at the interface is slow (exemplified by a low surfactant's desorption rate constant of 0.01 s^{-1}), the solution and the surface diffusion processes are essentially decoupled and proceed largely independently of each other. To demonstrate that this is indeed true, we used DigiSim, a commercially available electrochemical simulation software package created to exclusively model processes unperturbed by surface partitioning, to separately obtain the solution and surface cyclic voltammograms for the conditions of the lower left corner of Figure 3. We note that cyclic voltammograms obtained with line electrodes controlled by linear diffusion of redox species in 2D are equivalent to those obtained with planar electrodes and controlled by linear diffusion of redox species in 3D.[19,25] The comparison of the DigiSim[34] and our FEMLAB simulations in Figure 4 shows excellent agreement between the two for the solution processes. The peak currents in the two cases are 27.6 nA (DigiSim) and 27.4 nA (FEMLAB). The peak currents of the oxidation branch of the surface cyclic voltammogram also show excellent, ca. 1%, agreement: 0.357 nA (DigiSim) and 0.361 nA (FEMLAB). However, the reverse peak current of our FEMLAB simulation is ca. 10% smaller than that for the DigiSim surface diffusion case unperturbed by the surfactant's desorption. This is due to a small, yet finite rate of desorption of the oxidized surfactant in this slow scan voltammetric run.

The increasing rate constant of a surfactant's desorption from the air/water interface has a very strong effect on the surface current. This is illustrated in Figure 5. An increase of k_{des} to 1 s^{-1} or higher values completely eliminates the reverse, reduction peak due to complete desorption of the oxidized form from the water surface.

Finally, a different way to illustrate the effect of the increasing rate of a surfactant's equilibration at the air/water interface (increasing k_{des}) is to examine solution mass transport processes near the microband electrode. Pronounced effects are observed when D_{surf} is greater than D_{sol}. We illustrate this for the case of $D_{surf}/D_{sol} = 20$ in Figure 6. Shown there are two concentration profiles of TEMPO at the positive potential limit of the oxidation scan that were obtained for two substantially different k_{des} values of 10^{-2} and 10^2 s^{-1}. The substantially broader and asymmetric depletion of the solution next to the microband electrode is observed for the higher rate of adsorption/desorption at the air/water interface. This phenomenon is directly related to the existence of two channels of TEMPO diffusion to the microband: the first one, a hemicylindrical, solution channel of smaller D value, and the second, a linear, surface diffusion channel characterized by a higher value of D. In the case shown

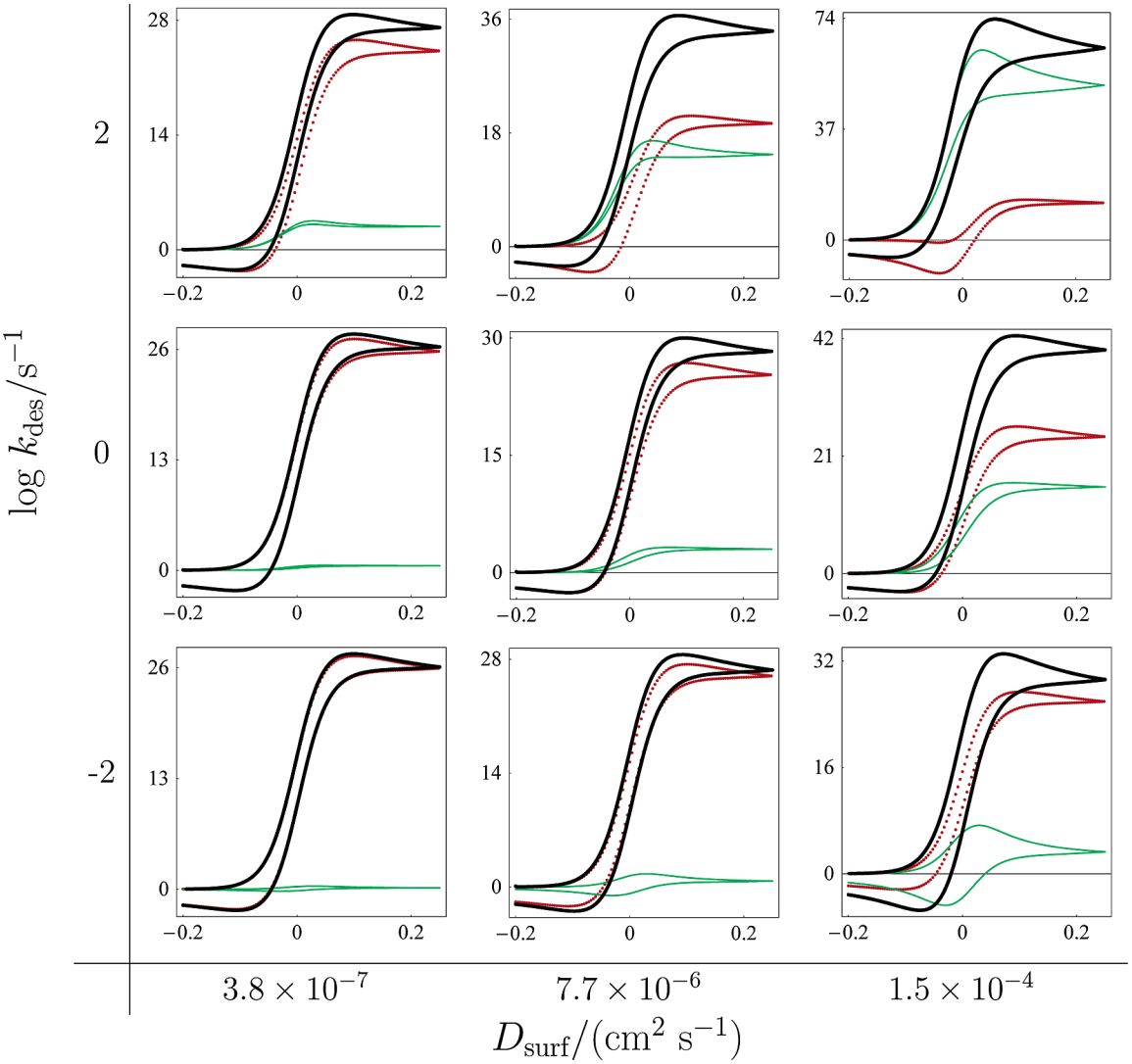

Figure 3. Set of simulated cyclic voltammograms obtained with a 100 nm wide, 1.0 cm long microband electrode positioned at the surface (zero meniscus height) of a $C_{init} = 0.10$ mM TEMPO solution for nine pairs of desorption rate constants (k_{des}) and surface diffusion constants. D_{surf} of 7.7×10^{-6} cm^2/s equals TEMPO D_{sol} value. The TEMPO partition constant is 5.0×10^2 M^{-1}. The voltammetric scan rate is 20 mV/s. The black, red, and green curves correspond to the total, solution, and surface currents, respectively (with the exception of the upper right corner, the solution current is always greater than the surface current). In each case, the current is given in nA and the potential is in V vs E^0.

in Figure 6B, efficient coupling between the two channels directs a substantial fraction of TEMPO flux via the surface channel. This results in the observed broadening of the solution concentration profile of TEMPO. This also results in the increase of the surface current and the decrease of the solution current relative to the total current with increasing k_{des} (see Figure 3 for $D_{surf} = 1.5 \times 10^{-4}$ cm^2/s). This is not observed in the case of Figure 6A where kinetics of the adsorption/desorption are assumed to be slow. The apparent asymmetric shape of the broadened concentration profile (Figure 6B) with respect to the position of the microelectrode is due to the fact that the air/water interface is located only on one side of the microband electrode (for $x > w$, see Figure 2). In other words the thickness of the glass slide supporting the microband electrode is effectively infinitely thick.

Experimental Results and Discussion

Effect of the Meniscus Height. Even a cursory examination of Figures 1 and 2 suggests that the height of water meniscus adjacent to the microband electrode might affect the magnitude of the solution current. To investigate this, the experiments were done with 4-hydroxy-TEMPO (OH−TEMPO), a derivative which does not partition to the air/water interface. To control the meniscus height (h), the edge of a microband electrode was first carefully aligned with the water surface. Then the electrode was lowered into contact with the water surface using a precision height gauge (see the Experimental Section). At that point, zero meniscus height (flat interface) was achieved. Next, the electrode was gradually lifted up and cyclic voltammograms were recorded as a function of the meniscus height. These are shown in Figure 7A for h in the range of 0−1778 μm. The highest achievable meniscus is ca. 1800 μm. Perhaps not surprisingly, the recorded current decreases as the meniscus height increases. To quantitatively understand the decrease, we expressed the meniscus height by the angle Θ formed between a linearized meniscus and the horizontal line, as shown in the inset in Figure 7A. Thus, a flat meniscus corresponds to $\Theta = 0°$. It is apparent that Θ is a parameter defining the fraction of the initially hemicylindrical volume of the solution within which solution mass transport processes evolve during the electrochemical experiments of Figure 7A. For example, we expect that $\Theta = 45°$ should correspond to the conditions yielding an OH−TEMPO oxidation current of three-quarters of the maximum value obtained at the flat meniscus with $\Theta = 0^o$. This is because

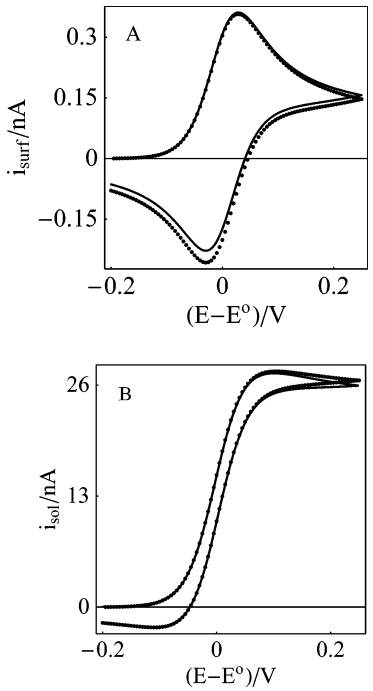

Figure 4. Comparison of the simulated voltammograms due to the surface (A) and solution (B) processes corresponding to $D_{surf} = 3.8 \times 10^{-7}$ cm^2/s and $k_{des} = 10^{-2}$ s^{-1} (lower left corner of Figure 3). All other parameters of the simulations are the same as those in Figure 3. In both parts, the continuous line curves correspond to the FEMLAB simulations and the dotted lines to the DigiSim simulations. FEMLAB simulations take into account surface partitioning phenomena. DigiSim simulations do not.

45° is one-quarter of 180°. Next we attempted to relate Θ and *h* using an equation holding for a Wilhelmy plate, a commonly used tool for measuring surface tensions. This equation relates the contact angle (ϕ) of a solution at a Wilhelmy plate to the meniscus height:[35]

$$\sin \phi = 1 - \frac{h^2 \Delta\rho g}{2\gamma} \tag{7}$$

where $\Delta\rho$ is the difference between the water and air densities, γ is the solution surface tension, and g is the gravitational acceleration. As defined above, $\Theta = 90 - \phi$. However, since eq 7 concerns the true contact angle at a Wilhelmy plate, we do not necessarily expect that the two angles are exactly equivalent. Nevertheless, eq 7 allowed us to obtain the values of Θ corresponding to the experimental values of the meniscus height of Figure 7A. Those were then used to generate a set of simulated voltammograms corresponding to those shown in Figure 7A. Naturally, our FEMLAB simulation code assumed no surface partitioning of OH−TEMPO or OH−TEMPO$^+$. The simulated voltammograms are shown in Figure 7B. As expected, the simulated voltammograms exhibit slightly lower peak currents that their experimental counterparts. This is also shown in Figure 8 where the correlations between the experimental and simulated plateau currents, the apparent meniscus angles, and the meniscus heights are shown. We conclude that a nearly perfect linear correlation exists between the observed plateau current and both the apparent meniscus angle Θ and the measured meniscus height. All experimental data involving TEMPO presented below were obtained at $\Theta = 0$.

TEMPO Surface Diffusion Constant. The FEMLAB simulation code described above was used to interpret the experimentally obtained cyclic voltammograms of TEMPO and

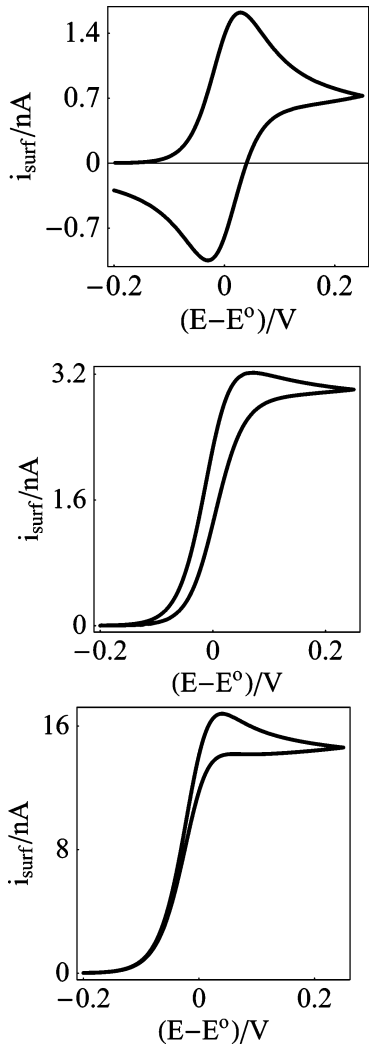

Figure 5. FEMLAB simulations of the surface current obtained for the increasing values of k_{des}, top to bottom, 10^{-2}, 1, and 10^2 s^{-1}. $D_{surf} = 7.7 \times 10^{-6}$ cm^2/s. All other parameters are the same as those in Figure 3.

TEMPO$^+$. The partition constants of both compounds were measured to be 504 ± 70 M^{-1} and 41 ± 3 M^{-1}, respectively. In view of a small value of K_{T^+}, we assumed that surface partitioning of TEMPO$^+$ can be neglected. Figure 9 shows typical cyclic voltammograms of TEMPO and TEMPO$^+$ each recorded with a microband electrode touching the water surface (50 mM $LiClO_4$, 1.0 mM $HClO_4$ solution). The reproducibility of the plateau current expressed as standard deviation of 11 separate experiments done with TEMPO concentrations of 0.10 and 0.025 mM is ±5%. While the concentrations and the solution diffusion constants of TEMPO and TEMPO$^+$ in their respective solutions featured in Figure 9 were identical, the plateau current in the TEMPO oxidation experiment is substantially greater than the plateau current in the TEMPO$^+$ reduction experiment. Furthermore, the latter voltammogram can be fit well with a simulation that assumes only solution mass transport. Clearly, partitioning of TEMPO$^+$ to the air/water surface is indeed negligible. It is likewise clear that kinetically facile partitioning of TEMPO to the air/water interface and its rapid surface lateral diffusion greatly increase the observed total current (recall that $i_{tot} = i_{sol} + i_{surf}$).

The quality of the fits can be assessed on the basis of the comparisons given in Figure 9. Decreasing TEMPO solution concentration 4-fold does not deteriorate the quality of the fit

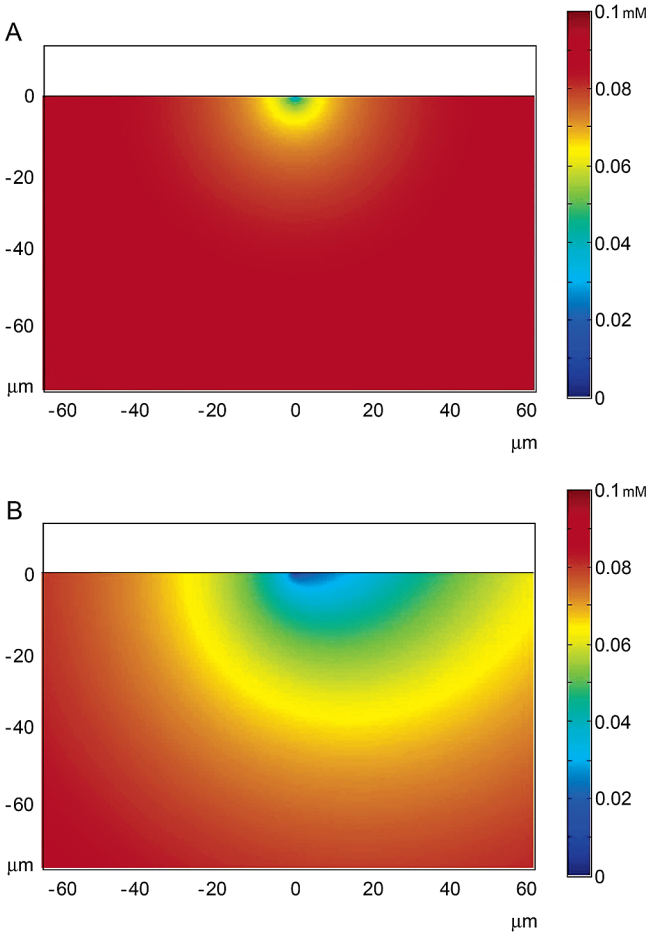

Figure 6. Two TEMPO solution concentration profiles existing at $E = 0.25$ V vs E^0, or at the end of a 20 mV/s anodic scan (see Figure 3), obtained for $D_{surf} = 1.5 \times 10^{-4}$ cm^2/s and k_{des} of 10^{-2} s^{-1} (A) and 10^2 s^{-1} (B). A 100 nm wide microband electrode is positioned in the middle of the top edge of each diagram (0, 0 point). The initial, bulk concentration of TEMPO is 0.1 mM.

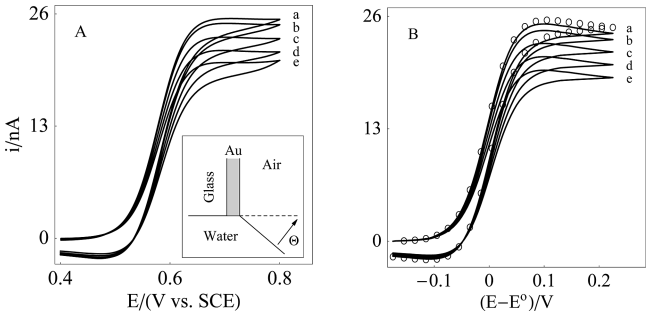

Figure 7. Set of experimental (A) and simulated (B) cyclic voltammograms of a 0.1 mM OH−TEMPO solution recorded at 20 mV/s with a 100 nm wide, 1.0 cm long microband electrode positioned at the air/water interface. The experimental voltammograms (A) were obtained with the meniscus height of (a) 0, (b) 254, (c) 762, (d) 1270, and (e) 1778 μm. The simulations (B) were done using a code that assumes no surface partitioning of the redox species. The values of the angle Θ used in the simulations (see inset in A) were (a) 0°, (b) 6°, (c) 16°, (d) 27°, and (e) 39°. Our FEMLAB simulations are drawn with the continuous line. For comparison, simulation (a) was also done with DigiSim (ref 34). It is marked with open circles.

involving the same parameters other than C_{init}. However, in most cases, we systematically observed a small discrepancy between the shape of the simulated and experimentally recorded TEMPO voltammograms in the most positive range of potentials. This discrepancy, a higher experimental current at $E > 0.6$ V, cannot

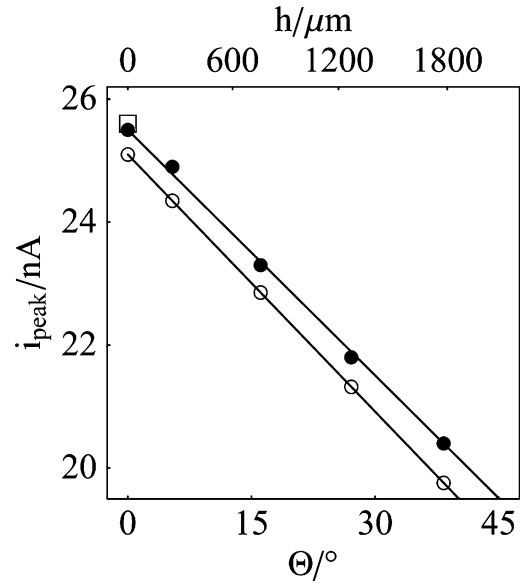

Figure 8. Correlation plot of the peak current, the meniscus height, and the angle Θ. Closed and open circles correspond to the experimental and simulated peak currents of Figure 7, parts A and B, respectively. The open square datum is the peak current of the DigiSim simulation (ref 34) in Figure 7B.

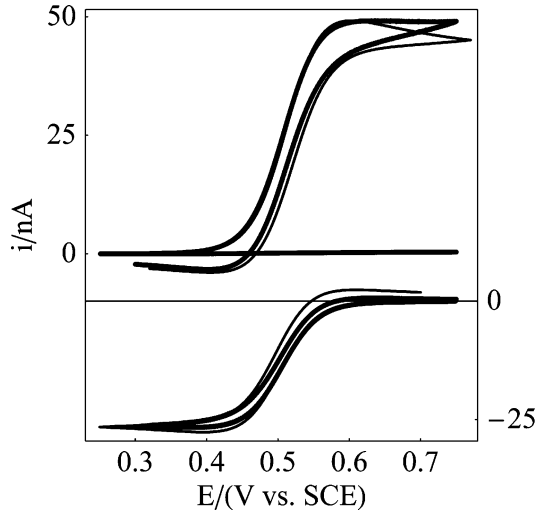

Figure 9. Cyclic voltammograms of TEMPO (top) and TEMPO$^+$ (bottom) recorded with a 100 nm wide, 1.0 cm long microband electrode touching the water surface (0.10 mM TEMPO or TEMPO$^+$, 50 mM $LiClO_4$, 1.0 mM $HClO_4$ solution); zero meniscus height; scan rate, 20 mV/s. Recorded currents are marked with a heavy continuous line (including background current in the top panel). FEMLAB simulations are drawn with a thin continuous line. Additional parameters of the simulations are listed in the caption of Figure 3. The measured formal potential of TEMPO$^{0/+}$ is 0.49 ± 0.01 V vs SCE. The values of D_{surf} and k_{des} used in the simulation of the TEMPO voltammogram are shown in Figure 10 and discussed in the text.

be eliminated by background subtraction. The latter is very small and invariant with potential as shown in Figure 9. It was, therefore, not subtracted from the recorded TEMPO voltammograms. It is plausible that the presence of TEMPO in solution has a small catalytic effect on electro-oxidation of the gold surface or water. Unfortunately, we are not able to confirm this hypothesis. This small discrepancy notwithstanding, we judge the fits between the experimental and simulated voltammograms to be very good.

As outlined in the Theoretical Description and Results section, simulations of TEMPO voltammograms such as the one in

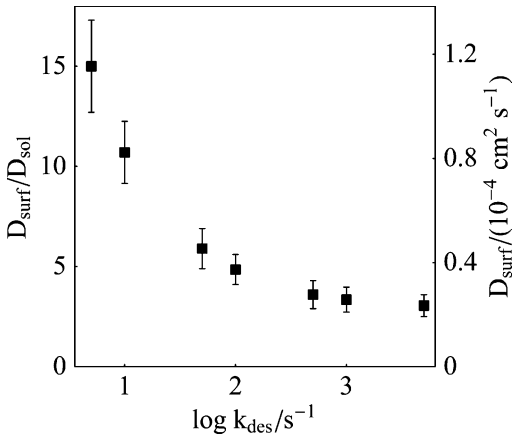

Figure 10. Calibration plot of D_{surf}/D_{sol} and D_{surf} vs log k_{des} ($D_{sol} = 7.7 \times 10^{-6}$ cm^2/s) obtained on the basis of the FEMLAB simulations and fitting of the total current to the average current of TEMPO electrooxidation of Figure 9. The error bars reflect 95% confidence intervals obtained on the basis of 11 voltammetric experiments with 0.10 and 0.025 mM TEMPO solutions.

Figure 9 require two adjustable parameters, D_{surf} and k_{des}. The relationship between the two obtained from several simulations fitting the TEMPO voltammogram such as that in Figure 9 is presented in Figure 10. This working curve can serve to determine one of the two parameters once the other becomes known or when it can be estimated. Thus, for example, if we take the expected value of TEMPO desorption rate constant to be in the range of $10-100$ s^{-1}, then its D_{surf} is in the range of $7.9-3.6 \times 10^{-5}$ cm^2/s. The error bars included in Figure 10 reflect the experimental precision of the recorded TEMPO oxidation currents. We did not systematically investigate the effect of scan rate. Application of significantly slower scan rates may be inconsistent with the assumption of the linear diffusion governing lateral mass transport of TEMPO on the water surface (see eq 4). We are also aware of the increasing effect of surface and bulk convection under the slow scan rate conditions. On the other hand, we determined that experiments carried with line microelectrodes at scan rate, $\upsilon \geq 100$ mV/s may result in lower $i/(\upsilon^{1/2}l)$ values. We discussed this in our previous report.[36] As mentioned above, the same fitting parameters were also obtained in the experiments carried out with a lower TEMPO concentration of 0.025 mM. Those together with 0.10 mM correspond to surface mean molecular areas of 4100 and 1100 Å^2/molecule, respectively. The independence of D_{surf} of the TEMPO surface concentration ensures us that the D_{surf} value that can be deduced from Figure 10 is not affected by the dynamics of TEMPO lateral intermolecular collisions. Finally, we note that our previous experimental strategy in which we assumed that the solution current can be recorded independently and then subtracted from the total current led to a larger average value of D_{surf} of 1.5×10^{-4} cm^2/s. As we pointed out then, our earlier methodology was correct only in the limit of a negligible rate of surface partitioning of TEMPO at the air/water interface. The current approach is free of this limitation.

Conclusions

To support our investigations of the dynamics of lateral diffusion of amphiphilic molecules at the air/water interface, we have developed a simulation code, using the FEMLAB platform, capable of generating cyclic voltammograms for redox systems in which one or both redox forms partition to the air/water interface and which are thus able to diffuse both in the bulk of the solution and along the air/water interface to a microband electrode positioned at that interface. The microband functions as a line electrode for the surface population of the redox species which are assumed to obey linear diffusion equations modified by the adsorption and desorption kinetics. In view of the narrow width of the microband (100 nm), the solution population exhibits hemicylindrical diffusion which may be significantly modified by the dynamics of solution/surface equilibration and transport. In view of the complexity of the transport phenomena involved in this class of systems, reliable current−voltage curves can be generated once the parameters characterizing the system's behavior in the solution and at the interface are known. These are the partition constant, rate of desorption or adsorption, and the diffusion constants of each redox form both at the air/water interface and in the solution. The heterogeneous electron-transfer rate constant must be also specified or assumed to be sufficiently high to render the electrochemical reactions diffusion controlled. We assumed that both the electron-transfer rate constant and the formal potential are the same for both surface and solution populations. The major results of the simulations were presented in Figures 3 and 10. We determined that the kinetics of partitioning at the air/water interface as well as the ratio of the surface and solution diffusion constants are the key parameters governing the behavior of this class of systems and, specifically, the magnitude of the total voltammetric current. The first of these determines the extent of coupling of the transport processes involving in the two transport domains, the interface and the solution. Under conditions of facile surface partitioning kinetics and a large ratio of D_{surf}/D_{sol}, substantial distortions of the solution transport can be observed as a result of the coupling.

We then relied on the capability to generate voltammetric simulations to interpret the experimentally recorded voltammograms of TEMPO redox processes at and near the air/water interface. Our independent characterization of the TEMPO/TEMPO$^+$ couple allowed us to generate cyclic voltammograms with just two adjustable parameters, TEMPO D_{surf} and k_{des}. By fitting the recorded line/microband electrode voltammograms, we constructed a calibration curve D_{surf} versus k_{des} covering a full range of physically realistic and relevant desorption rate constants (see Figure 10). Once the latter becomes known, the calibration curve may be used to obtain the lateral surface diffusion constant of TEMPO. An experimental determination of that rate is one option that we currently pursue. The other involves an assertion that TEMPO derivatives with a short alkane chain (such as ethyl, butyl, hexyl) attached to the carbon atom of the piperidine ring opposite the nitroxide group will exhibit identical surface diffusion constants. This assertion is supported by the electronic structure calculations showing that the TEMPO water interactions are limited to hydrogen bonding of one or two water molecules by the oxygen of the nitroxide group leaving the entire TEMPO molecule unimmersed in water.[18] We expect that the 4-alkane-TEMPO derivatives will progressively exhibit larger partition constants and that, therefore, their total oxidation current will be increasingly dominated by the surface current. Once these expectations are experimentally confirmed, we will be able to simultaneously interpret our electrochemical data both in terms of both D_{surf} and the desorption rate constants of these amphiphiles.

Acknowledgment. We acknowledge and thank Professor Clayton J. Radke for helpful discussions of interfacial transport processes at the early stage of this project. This work was supported by the National Science Foundation under Grants CHE-0416349 (M.M.) and CHE-0315558 (M.V.M.). We also acknowledge the donors of the Petroleum Research Fund,

administered by the American Chemical Society, for partial support of this research.

References and Notes

(1) Richmond, G. L. *Chem. Rev.* **2002**, *102*, 2693−2724.
(2) Richmond, G. L. *Annu. Rev. Phys. Chem.* **2001**, *52*, 357−389.
(3) Allen, H. C.; Raymond, E. A.; Richmond, G. L. *Curr. Opin. Colloid Intface Sci.* **2000**, *5*, 74−80.
(4) Miranda, P. B.; Shen, Y. R. *J. Phys. Chem. B* **1999**, *103*, 3292−3307.
(5) Eisenthal, K. B. *Chem. Rev.* **1996**, *96*, 1343−1360.
(6) Braslau, A.; Pershan, P. S.; Swislow, G.; Ocko, B. M.; Als-Nielsen, J. *Phys. Rev. A* **1988**, *38*, 2457.
(7) Braslau, A.; Deutsch, M.; Pershan, P. S.; Weiss, A. H. *Phys. Rev. Lett.* **1985**, *54*, 11, 4−117.
(8) Wilson, K. R.; Schaller, R. D.; Co, D. T.; Saykally, R. J.; Rude, B. S.; Catalano, T.; Bozek, J. D. *J. Chem. Phys.* **2002**, *117*, 7738−7744.
(9) Maroncelli, M.; Fleming, G. R. *J. Chem. Phys.* **1988**, *89*, 5044−5069.
(10) Townsend, R. M.; Rice, S. A. *J. Chem. Phys.* **1991**, *94*, 2207−2218.
(11) Pohorille, A.; Wilson, M. A. Viewpoint 9—Molecular Structure of Aqueous Interfaces. *J. Mol. Struct. (THEOCHEM)* **1993**, *284*, 271−298.
(12) Benjamin, I. *Phys. Rev. Lett.* **1994**, *73*, 2083.
(13) Taylor, R. S.; Dang, L. X.; Garrett, B. C. *J. Phys. Chem. B* **1996**, *100*, 11720−11725.
(14) Dang, L. X.; Chang, T.-M. *J. Chem. Phys.* **1997**, *106*, 8149.
(15) Sokhan, V. P.; Tildesley, D. J. *Mol. Phys.* **1997**, *92*, 625−640.
(16) Liu, P.; Harder, E.; Berne, B. J. *J. Phys. Chem. B* **2005**, *109*, 2949−2955.
(17) Wick, C. D.; Dang, L. X. *J. Phys. Chem. B* **2005**, *109*, 15574−15579.
(18) Wu, D. G.; Malec, A. D.; Head-Gordon, M.; Majda, M. *J. Am. Chem. Soc.* **2005**, *127*, 4490−4496.
(19) Majda, M. Electrochemistry of Monolayer Assemblies at the Air/Water Interface. In *Encyclopedia of Electrochemistry*; Bard, A. J., Stratman, M., Eds.; Wiley-VCH: Weinheim, Germany; Vol. 10, Chapter 4, in press.
(20) Bobbitt, J. M.; Flores, M. C. L. *Heterocycles* **1988**, *27*, 509−533.
(21) Bobbitt, J. M.; Flores Guthermuth, M. C.; Ma, Z.; Ta, H. *Heterocycles* **1990**, *30*, 1131−1140.
(22) Bobbitt, J. M. *J. Org. Chem.* **1998**, *63*, 9367−9374.
(23) Golubev, V. A.; Zhdanov, R. I.; Gida, V. M.; Rozantsev, E. G. *Bull. Acad. Sci. USSR, Div. Chem. Sci.* **1971**, *20*, 768−770.
(24) Johnson, M. J.; Anvar, D. J.; Skolimowski, J. J.; Majda, M. *J. Phys. Chem. B* **2001**, *105*, 514−519.
(25) Johnson, M. J.; Majmudar, C.; Skolimowski, J. J.; Majda, M. *J. Phys. Chem. B* **2001**, *105*, 9002−9010.
(26) Hyk, W.; Ciszkowska, M. *J. Phys. Chem. B* 1999, *103*, 6466−6474.
(27) Zhang, W.; Ma, C.; Ciszkowska, M. *J. Phys. Chem. B* **2001**, *105*, 3435−3440.
(28) Britz, D. *Digital Simulation in Electrochemistry*, 2nd ed.; Springer-Verlag: Berlin, 1988; pp 40−42.
(29) Fish, J. R.; Swarts, S. G.; Sevilla, M. D.; Malinski, T. *J. Phys. Chem.* **1988**, *92*, 3745−3751.
(30) Bard, A. J.; Faulkner, L. R. *Electrochemical Methods. Fundamentals and Applications*, 2nd ed.; J. Wiley & Sons: New York, 2001; Chapter 4.4.3, p 151.
(31) Radke, C. J.; MacLeod, C. A. *J. Colloid Interface Sci.* **1994**, *166*, 73.
(32) Joos, P.; Serrien, G. *J. Colloid Interface Sci.* **1989**, *127*, 97.
(33) Shin, J. Y.; Abbott, N. L. *Langmuir* **2001**, *17*, 8434−8443.
(34) Using DigiSim, to simulate a cyclic voltammogram at a microband electrode with a width w, one uses the hemicylindrical simulation mode defining the radius of the microcylinder as $r = w/4$.
(35) Adamson, A. W. *Physical Chemistry of Surfaces*, 4th ed.; J. Wiley and Sons, Inc.: New York, 1982; Chapter II-8, p 24.
(36) Wu, D. G.; Malec, A. D.; Majewski, J.; Majda, M. *Electrochim. Acta* **2006**, *51*, 2237−2246.